

RATNA SUNIL BURADAGUNTA^{1*}, B. VENKATESWARLU², AMBUJ SHARMA³,
 FEROUZ SHAIK¹, RAVIKUMAR DUMPALA⁴

CHARACTERIZATION, MECHANICAL AND CORROSION BEHAVIOR OF Mg-Sn-Pb ALLOY PRODUCED BY FRICTION SURFACE ALLOYING

The current paper demonstrates friction-assisted surface alloying to produce Mg-Sn-Pb alloy within the solid state by using friction stir processing (FSP) principle. A groove is machined on the surface of pure magnesium sheet and a thin wire of Sn-Pb was inserted into the groove and then FSP was carried out on the surface. In order to achieve uniformity in the alloy formation, second pass was also carried out on the stirred region. Development of Mg-Sn-Pb alloy was observed at the surface as reflected from the corresponding X-ray diffraction peaks. Surface micro-hardness of the produced surface Mg-Sn-Pb alloy was significantly increased than pure Mg. Corrosion behavior was assessed by polarization tests and the result indicated higher corrosion resistance for the produced alloy due to the developed solid solution grains. Both the first-pass and second-pass samples have exhibited similar levels of corrosion resistance. Higher tensile strength (148.7 ± 5.1 MPa) was observed for the produced surface alloy and second-pass marginally elevated the tensile strength (152.1 ± 3.8 MPa) compared with Mg (106.2 ± 4.2 MPa). Higher ductility was also observed as reflected from the increased % of elongation (7.4 ± 0.8 and 8.2 ± 1.1) for the produced alloys compared with Mg (4.3 ± 0.7). The present work demonstrates the potential of friction surface alloying to develop Mg-Sn-Pb alloy without melting the base material that exhibits improved corrosion and tensile properties. Furthermore, it is also concluded that the second pass marginally increases the corrosion and mechanical performance of the alloy.

Keywords: Magnesium; Surface alloying; Solid-state processing; Corrosion; Mechanical strength

1. Introduction

Developing highly hard and functional surfaces by modifying the surface composition or depositing coatings of appropriate phases on the substrate are the viable strategies in surface engineering to enhance the surface properties of the structures without affecting the core. On the other hand, alloying helps to develop metallic structures with improved properties and offers several benefits in engineering applications. Producing surface composites by dispersing different phases into the substrate without changing the chemical composition of the core is widely seen in materials engineering [1]. Special methods including centrifugal casting [2], surface laser melting [3], plasma spraying [4], friction stir processing (FSP) [1], friction surfacing (FS) [5] etc. are used to alter the phases at the surface of materials to introduce specific properties to the surfaces without altering the core of the structures. Among these methods, solid-state processes such as FSP reduce the limitations involved in the liquid-state methods [6].

FSP is employed to refine surface microstructure and also to produce surface composites by introducing reinforcements into the surface [7]. Usually, hard and brittle reinforcing phases which exhibit higher melting point than the substrate are selected. Therefore, the reinforcing phases remain in the solid state but subjected to stirring and mixing within the processed zone during FSP. The composite layer thickness is dependent of the grooves or holes filled with reinforcements at the surface and the FSP tool geometry [8]. A few process variations have also been documented in friction-assisted techniques to modify the metallic surfaces in order to impart unique features at the surface itself, leaving the interior of the structure unaffected. One such technique is called friction surfacing, in which the substance to be coated is transferred to a substrate by means of plastic deformation aided by heat produced by friction between the substrate and rotating consumable rod [9]. Dilip and Janaki Ram [10] demonstrated another process named as “friction deposition” in which layer-by-layer deposition of material from

¹ PRINCE MOHAMMAD BIN FAHD UNIVERSITY, DEPARTMENT OF MECHANICAL ENGINEERING, AL-KHOBAR 31952, SAUDI ARABIA

² RAJIV GANDHI UNIVERSITY OF KNOWLEDGE TECHNOLOGIES (AP-IIIT), DEPARTMENT OF METALLURGICAL AND MATERIALS ENGINEERING, NUZVID 521101, INDIA

³ SCHOOL OF MECHANICAL ENGINEERING, VIT-AP UNIVERSITY, AMARAVATI 522237, ANDHRA PRADESH, INDIA

⁴ VISVESVARAYA NATIONAL INSTITUTE OF TECHNOLOGY, DEPARTMENT OF MECHANICAL ENGINEERING, NAGPUR 440010, INDIA

* Corresponding author: bratnasunil@gmail.com, rburadagunta@pmu.edu.sa



a spinning consumable rod is transferred to a substrate which can be viewed as an additive manufacturing technique. The same group also developed a different method called “friction-free form” that uses layer deposition by friction to create 3D structures [11]. The two other variations “friction stir cladding” [12] and “friction stir channeling” [13], were also reported in the literature which are categorized as friction-assisted process to produce blind channels inside the solid and to deposit surface layers on the substrates, respectively.

Usually, the dispersing phases are not melted by the heat produced during FSP. However, if the dispersed phase is locally melted due to the heat produced during FSP, an alloy can be developed between the dispersing phase and the substrate. It has been shown that, at the right processing conditions, the temperature in the nugget zone is reached up to 0.7-0.8 times of the melting point of the substrate during FSP [14]. Therefore, the dispersing phase melting temperature must be lower than the matrix material (substrate) in order for the heat produced during FSP to cause the dispersing phase to melt and to produce a surface alloy. In the previous work, a binary surface alloy of Mg-Zn was successfully produced by “friction surface alloying” (FSA) and excellent corrosion resistance was observed against simulated body fluids [15]. FSA is differed with the friction surfacing process. In friction surfacing, the intended alloy to be deposited on the surface is used as consumable rod. In the proposed FSA process, alloy is developed *in situ* while the process is carried out. Developing surface alloys by using the principle of FSA is not widely seen in

the available scientific data. Hence, FSA was adopted in this work with an objective to produce Mg-Sn-Pb surface alloy by using pure Mg as the substrate and 60/40 Sn-Pb soldering wire as the dispersing phase. Then the produced surface alloy was characterized and the corrosion properties were evaluated and discussed.

2. Materials and methods

Pure Mg (99.9%) sheets ($100 \times 100 \times 4 \text{ mm}^3$) were purchased from Exclusive Magnesium, India. A groove measuring 2 mm in width and 2 mm in depth was machined into the pure Mg sheet, and 60/40 Sn-Pb wire (2 mm diameter) was placed inside the groove. The sheet was then fixed on a vertical milling machine table (Bharat Fritz Werner, India). An FPS tool (H13 steel) was employed to perform FSA at 1400 rpm (rotation speed) and 25 mm/min (travel speed) with zero tool tilt angle. The process parameters were selected based on the previous studies [15,16]. A tool with threaded taper pin profile was selected with a shoulder diameter of 20 mm. Threaded pin profile gives higher level of material mixing during the stirring of the tool and hence, threaded profile was selected [14]. The pin (5 mm length) has a diameter of 5 mm at the shoulder and 2 mm at the tip. The schematic illustration of FSA, photographs of Mg substrate, processing, and produced surface alloy are presented in Fig. 1. After completion of 1st pass, the surface alloy was subjected to 2nd pass. The samples were named as Mg, alloy 1

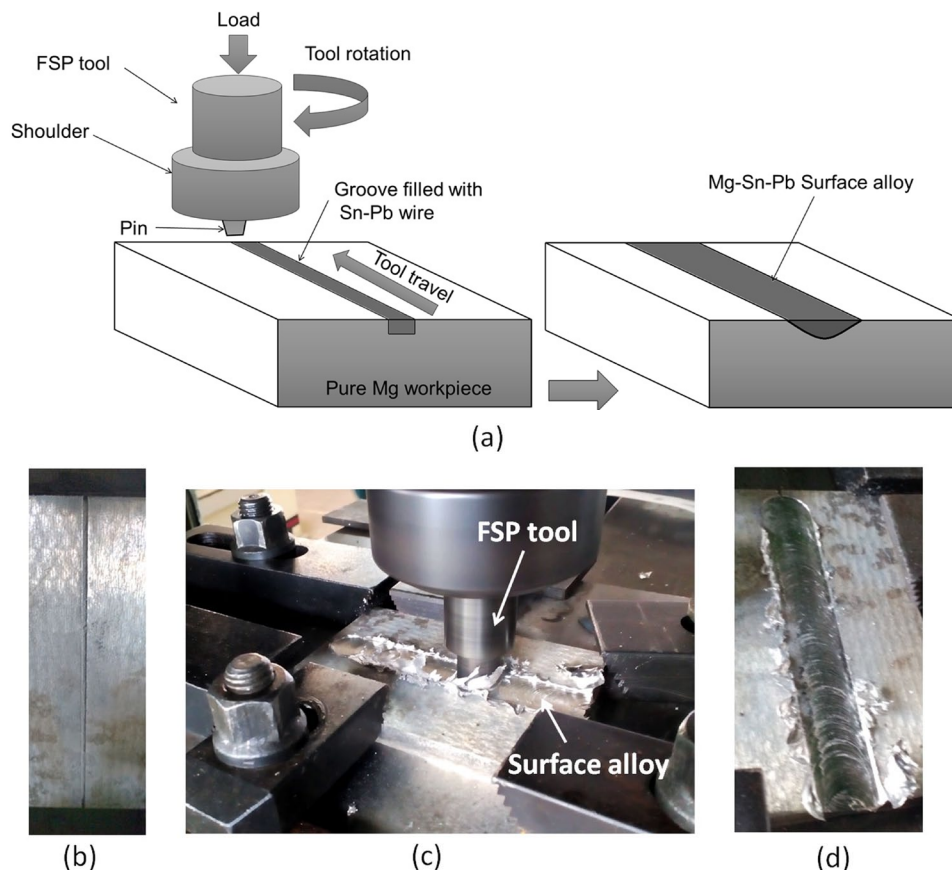


Fig. 1. (a) Schematic presentation of FSA process used to develop surface alloy of Mg-Sn-Pb, (b) photograph of the Mg substrate with groove, (c) surface alloying during the 2nd pass, (d) produced Mg-Sn-Pb surface alloy after 2nd pass

and Alloy 2 for pure Mg substrate, surface alloy after 1st pass of FSA and 2nd pass of FSA respectively.

Samples were extracted from the base material and also from the produced surface alloys. For microstructural examinations (Leica, Germany), polished samples with mirror finish were etched with Picral reagent [15]. From the microstructures, the average grain size was measured by linear intercept method in which lines of known length are drawn across the micrograph and the total intercepted grains are counted to obtain the average grain size [17]. The materials were analyzed by using X-ray diffraction (XRD, D8 Bruker, USA) between 20° to 80° range. Microhardness (Omnitech, India, 100 g load for 15s) was measured on the surface and at the cross-section of the produced alloys and compared with the Mg substrate. Measurements were recorded in the thickness direction of the cross-section and across the stir zone of the produced surface alloys.

The corrosion experiments were done by using 3.5% NaCl solution through polarization studies (IVIUM Soft, Netherlands). Workpiece was considered as the “working electrode” and platinum electrode was used as counter in the presence of saturated calomel electrode (reference electrode). Initially, cell potential was stabilized for 30 min and then polarization experiments were carried out between the fixed range of potential (–1000 to 1000 mV) with 5 mV/s scan rate. Electrochemical parameters were then recorded using Tafel extrapolation of the polarization curves of the samples [18]. In order to record the corrosion parameters, from the polarization curves, the change from anodic polarization to cathodic polarization is noted as corrosion

potential (E_{corr}). Then the tangents are drawn from the anodic and cathodic branches from the point where slope is significantly changed. The corresponding value of the intersection point on the horizontal axis gives the corrosion current density (i_{corr}). From the obtained i_{corr} values, corrosion rate (CR) was calculated by using Eq. (1).

$$CR \text{ (mm/year)} = 0.0254 \times 0.129 \times a \times i_{corr} / nD \quad (1)$$

Where, a is molar mass of Mg (24.3 g/mol), n is the valance (2) and D is the density (1.74 g/cm³) of Mg. After the polarization studies, the corroded sample surfaces were subjected to scanning electron microscopy (SEM, Carl ZEISS, Germany) to investigate the surface morphologies. For tensile experiments (Zwick/Roell, Germany), sub-size test samples ($n = 2$) as per ASTM-E8 standards [19] were prepared by wire EDM. Tensile samples were cut from the surface alloys and the Mg substrate. The surfaces of the test samples were polished to remove the surface unevenness and then experiments were carried out at the ambient conditions by employing 0.01/s strain rate. From the stress-strain curves, tensile properties were measured and compared.

3. Results and discussion

The surface alloy exhibited distinctive microstructure in the processed region compared with the core of the base alloy. Fig. 2 presents the microstructures of the Mg and the surface alloys. It is evident that the process resulted fine grained surface.

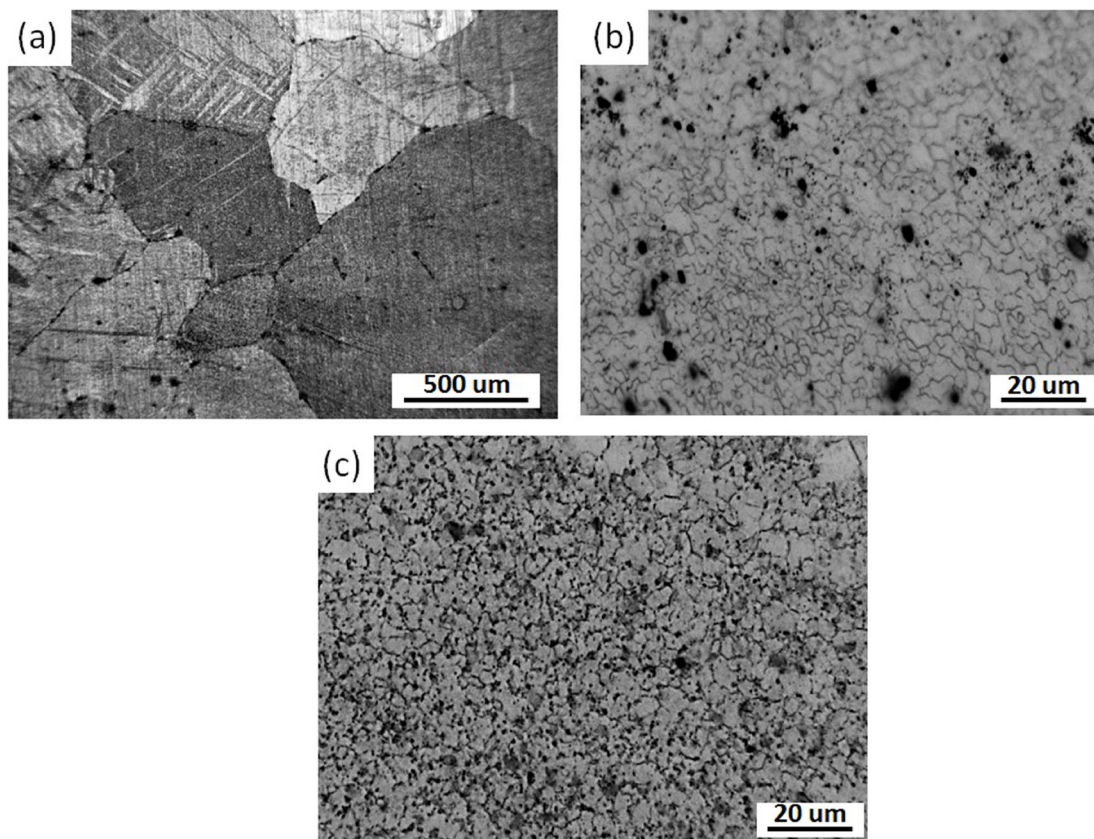


Fig. 2. Microstructures of the samples: (a) pure Mg, (b) Alloy 1 (Mg-Sn-Pb alloy after 1st pass) and (c) Alloy 2 (Mg-Sn-Pb alloy after 2nd pass)

From $\sim 1500 \mu\text{m}$, significant grain refinement up to $2.7 \pm 2.5 \mu\text{m}$ and $2.1 \pm 1.4 \mu\text{m}$ was observed in the surface alloy after 1st pass and 2nd pass respectively. Relatively, smaller grain size was observed in the surface alloy after 2nd pass. Several intermetallic particles were also appeared (as confirmed by XRD analysis) in the surface alloy as distributed across the processed region. After 2nd pass, the intermetallic particle size was observed as decreased. Fig. 3 presents the XRD patterns of pure Mg and the developed surface alloys after 1st pass and 2nd pass. The peaks were indexed by referring to the standard XRD data (ICDD, "International Center for Diffraction Data"). The XRD of the surface alloy confirms the development of intermetallics Mg_2Sn (JCPDS No. 31-0812) and Mg_2Pb (JCPDS 01-0465) in the surface alloy after 1st pass. By referring to the binary phase diagram of Mg-Sn alloy, it is understood that the solubility of Sn is maximum (14.48%) at 561.2°C and significantly decreases to less than 1% at room temperature [20]. Similarly, in the binary alloy of Mg-Pb, the maximum solubility of Pb (7.75%) in Mg can be observed at 466.2°C and with the decreased temperature, the solubility is drastically decreased to less than 1% [21]. Usually in the binary alloys, development of intermetallics is inevitable if the alloying element exceeds the solubility limit. Therefore, the development of Mg_2Sn and Mg_2Pb intermetallics is expected, since more amount of Sn and Pb was available in the stir zone. Interestingly, the peaks corresponding to these intermetallics were disappeared after 2nd pass which is an indication to the decreased amount of intermetallics due to 2nd pass FSA. Both the surface alloys (1st pass and 2nd pass) have exhibited similar peak intensities. The intensity of (002) peak was considerably increased in the surface alloys compared with Mg which is an indication of development of basal dominated texture in the surface alloys. Both the microstructural studies and XRD analysis confirm the smaller grains and basal dominated texture in the produced surface alloys. Additionally, 2nd pass alloy exhibits decreased intermetallics that suggest the development of supersaturated grains [22-24]. Basal planes (002) are high density planes

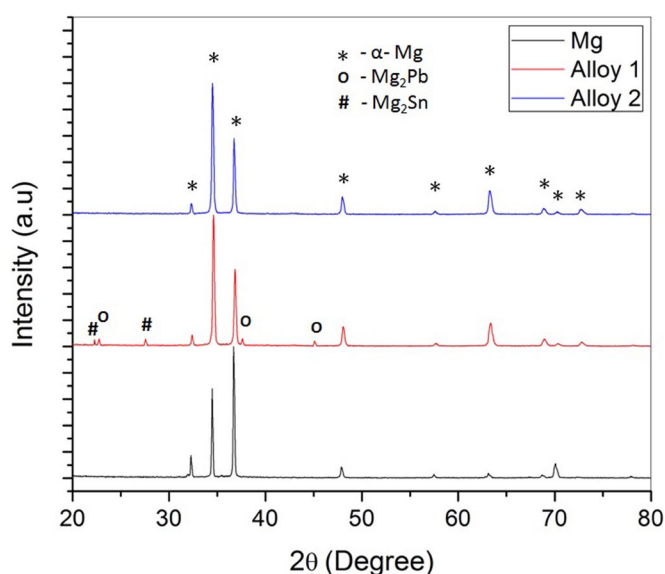


Fig. 3. XRD patterns of the samples

which exhibit lower affinity of chemical reaction and results in higher corrosion resistance. Therefore, the development of basal dominated texture in the surface alloy promotes the corrosion resistance. After 2nd pass, the texture development was similar to that of the 1st pass alloy and hence, similar level of corrosion resistance is expected in both the surface alloys.

In developing surface composites by FSP, increasing the number of passes may help to achieve uniform distribution of the reinforcing phases into the substrate [14]. Whereas in the surface alloying, the incorporated dispersing phase is intended to be melted and dissolved into the matrix. Increased number of passes alters the solubility of the added alloying element within the stir zone. However, microstructural changes can be expected with the increased number of passes in FSP [25]. The increased number of passes also increases the grain refinement level and brings the uniformity in the grain size. The uniformity in the alloy formation at the surface is also increased with the number of passes. In the present work, marginally decreased grain size was measured in the 2nd pass sample compared with the 1st pass sample in addition to the development of basal dominated texture which can influence the structure-dependent properties.

From the earlier works, the development of supersaturated grains by dissolving more solute into Mg matrix was demonstrated after FSP [22-24]. Hence, in the present work, dissolution of more Sn and Pb into Mg matrix can be observed after the 2nd pass. The surface alloy that is produced by FSA exhibits special characteristics including smaller grains rich with solute atoms and fine intermetallics. These special surface characteristics compared with the other liquid state methods make FSA as distinctive and promising in developing surface alloys with enhanced properties.

Microhardness measurements across the cross-section and on the produced surface alloy are presented in Fig. 4. The average hardness values of the surface alloys were measured as $86.2 \pm 7.4 \text{ HV}0.1$ and $93.2 \pm 4.2 \text{ HV}0.1$ for Alloy 1 and Alloy 2 compared with Mg ($41.8 \pm 4.5 \text{ HV}0.1$). It is evident that higher values were observed for the developed surface alloys. A drastic fall in the hardness can be seen at the interface of produced surface alloy and the Mg substrate. After 2nd pass, the variations within the hardness can be observed as decreased. Increased hardness was observed for the 2nd pass sample compared with the 1st pass sample. The increased hardness in the surface alloy is attributed to the benefit of the alloying effect compared with pure Mg.

Fig. 5 presents the polarization curves and TABLE 1 lists the obtained electrochemical parameters (E_{corr} and i_{corr}) from the polarization curves of the samples and the calculated corrosion rate of the samples. The surface alloys exhibited a clear distinction in the electrochemical parameters. Shifting the E_{corr} towards more positive values indicates the noble behavior of the produced alloys. Furthermore, lower i_{corr} values also indicate the improved corrosion resistance for the developed alloys compared with Mg. Smaller i_{corr} values observed for the surface alloys indicate lower current flow through the workpiece under varying potential in the presence of the corroding electrolyte

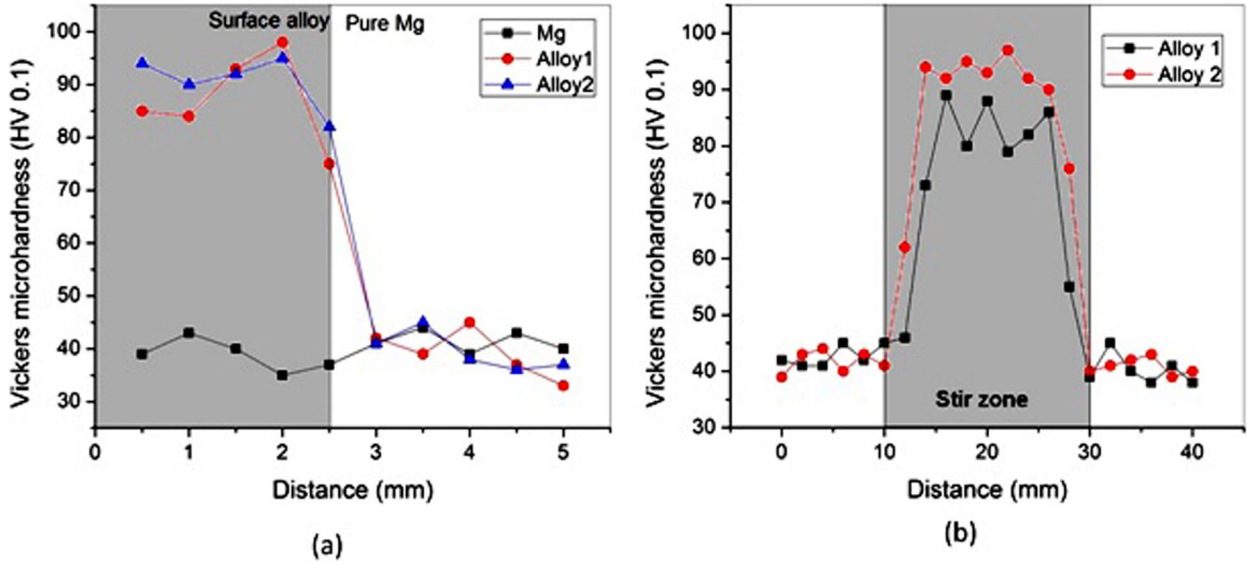


Fig. 4. (a) microhardness in the thickness direction at the cross-section and (b) across the stir zone of Alloy 1 (Mg-Sn-Pb alloy after 1st pass) and Alloy 2 (Mg-Sn-Pb alloy after 2nd pass)

which resulted in lower corrosion rates. Improved corrosion resistance for the surface alloys is attributed to the metallurgical benefit that is usually achieved in alloying by developing solid solution grains and smaller grains in the alloys. Decreased grain size increases the grain boundary and promotes quick passivation in the Mg alloy which enhances the corrosion resistance [26,27]. 2nd pass sample exhibited marginal improvement in the corrosion resistance compared with the 1st pass sample. This can

be ascertained to the effect of the decreased intermetallics size and volume which reduced the galvanic corrosion and also due to the decreased grain size.

Fig. 6 presents the scanning electron microscope images of the surfaces after the PDP tests. Compared with the surface alloys, pure Mg has shown regions of severe corrosion attack. Within the surface alloys, 2nd pass sample has shown lower surface degradation due to corrosion compared with the 1st pass sample. The surface morphologies show uniform corrosion for the 2nd pass sample due to the smaller grain size and higher uniformity in the grain size of 2nd pass sample compared with the 1st pass sample.

Fig. 7 shows the “stress-strain curves” obtained from the tensile tests and TABLE 2 lists the calculated tensile properties. Compared with pure Mg, the surface alloys have shown higher strength. Higher yield strength was recorded for the surface alloys compared with the base samples. By observing the ultimate tensile strength values, within the surface alloys, 2nd pass sample has shown marginally higher strength without deteriorating the % of elongation compared with the 1st pass sample. Interestingly, the ductility of the surface alloys was also observed as increased compared with the pure Mg sample. Usually, with the increased strength, the ductility of metals is decreased. However, due to the alloying, the formability and ductility of the metals can be successfully improved along with improving the load-bearing capacity. Therefore, the benefit of alloying Mg with Sn and Pb to enhance the strength can be seen for the developed surface alloys in addition to the improved ductility.

The present work exhibits the formation of Mg-Sn-Pb surface alloy by FSA without melting the substrate. Compared with the core of the substrate, improved corrosion and mechanical performance can be achieved in these surface alloys. Additionally, issues such as oxidation and development of undesired intermetallics from the solidification can be completely eliminated by adopting the solid-state method. It is noted that the

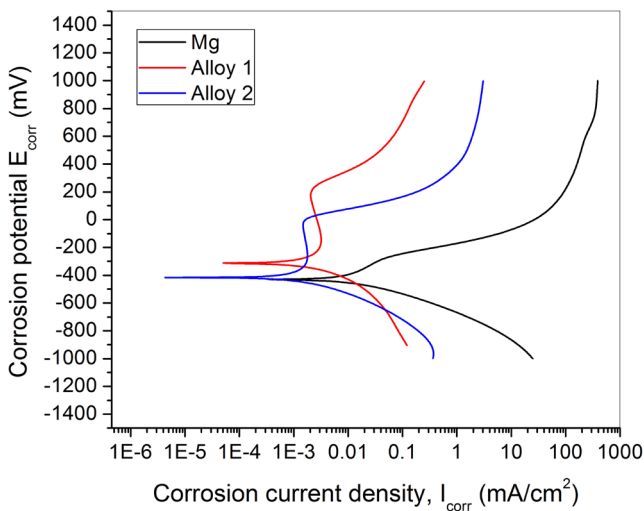


Fig. 5. Potentiodynamic polarization curves of the samples

TABLE 1

Corrosion parameters recorded from the polarization tests

Sample	Corrosion potential (E_{corr}) (V)	Corrosion current density (i_{corr}) (A/cm^2)	Corrosion rate (mm/year)
Pure Mg	-427	8.2×10^{-4}	18.76
Alloy 1	-319	0.99×10^{-4}	2.26
Alloy 2	-416	0.78×10^{-4}	1.78

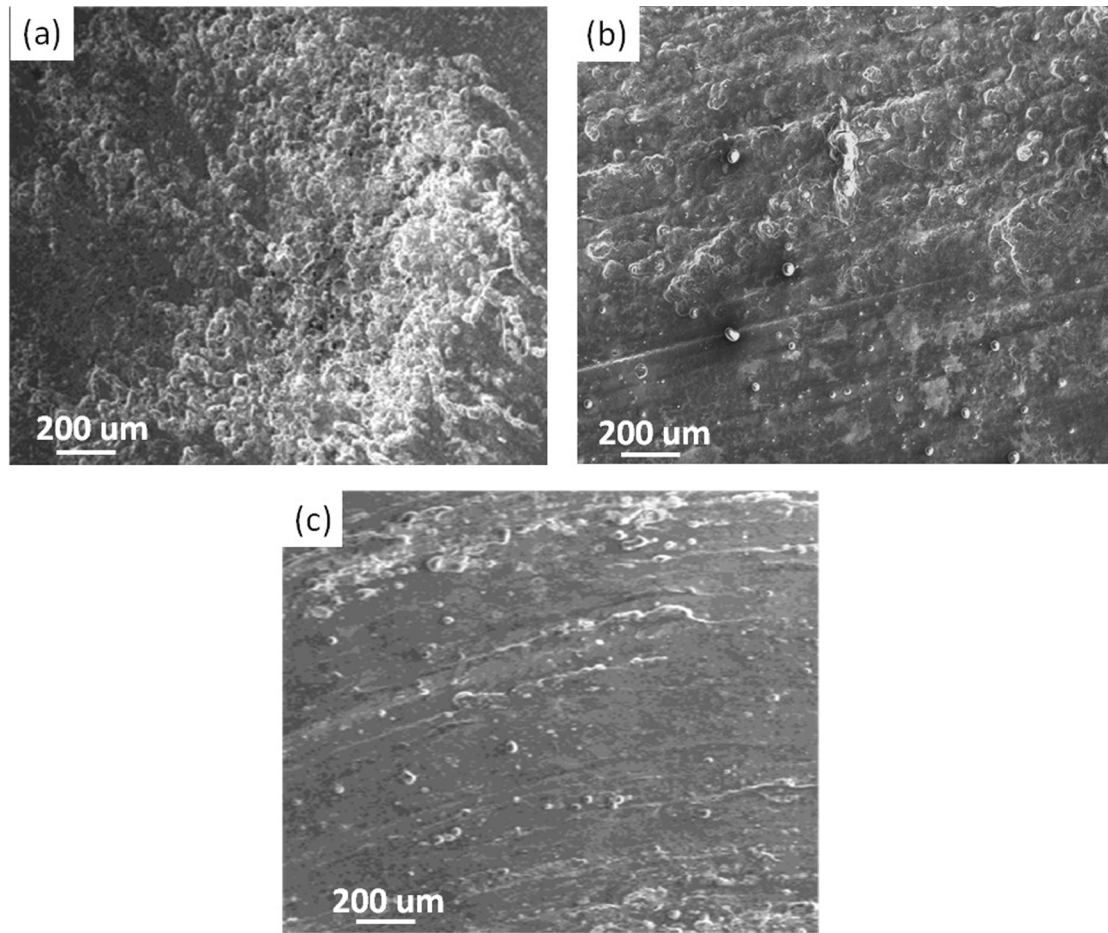


Fig. 6. Scanning electron microscope images of the surfaces after PDP test: (a) Mg, (b) Alloy 1 (Mg-Sn-Pb alloy after 1st pass) and (c) Alloy 2 (Mg-Sn-Pb alloy after 2nd pass)

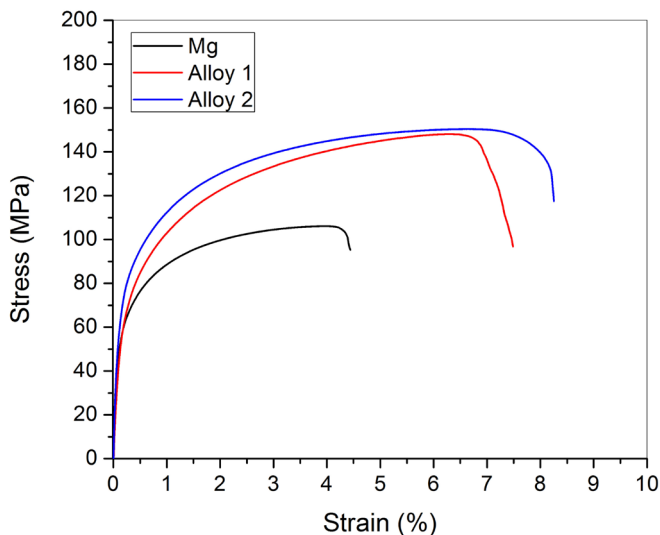


Fig. 7. Stress-strain curves of the samples

exhibited performance of the developed Mg-Sn-Pb alloy surface is inferior compared with the commercial grade Mg alloys such as AZ31, ZE41, WE43 etc. [28]. However, developing surface alloy without altering the core in solid state is technically challenging which is addressed in the current work. The preliminary results demonstrate the potential of developing surface alloys

TABLE 2

Tensile properties of the samples recorded from the stress-strain curves

Sample	Yield strength (MPa)	Ultimate tensile strength (MPa)	% elongation
Pure Mg	62.5 ± 2.1	106.2 ± 4.2	4.3 ± 0.7
Alloy 1	79.7 ± 2.5	148.7 ± 5.1	7.4 ± 0.8
Alloy 2	81.2 ± 3.3	152.1 ± 3.8	8.2 ± 1.1

with FSA. In order to produce surface alloy in FSA, the intended alloying element that is dissolved into the substrate must have lower melting temperature than that of the substrate. This is a limitation that restricts the choice of selection of alloying element. However, different combinations of reinforcements can be selected to develop solid-state surface alloys by FSA. Since the dissolution of alloying element into the surface is limited, adding higher alloying element is technically challenging by FSA. Furthermore, other surface properties of these solid-state surface alloys such as tribological properties, oxidation and degradation properties, interface strength, mechanical failure under different types of loading conditions etc are yet to be investigated. The feasibility of FSA to produce other surface alloys by using pure metals such as aluminium, titanium, zinc or their alloys as the substrates also needs to be explored.

4. Conclusions

Mg-Sn-Pb surface alloy was produced in the present work without melting the substrate by using friction surface alloying (FSA), a variant of friction stir processing in which the reinforcement is melted and dissolved into the substrate to produce the surface alloy. Sn-Pb wire was placed in a groove machined on the surface of a pure Mg plate and FSA was carried out up to 2 passes. Microstructural studies revealed grain refinement of $2.7 \pm 2.5 \mu\text{m}$ and $2.1 \pm 1.4 \mu\text{m}$ in 1st pass and 2nd pass samples, respectively compared with the pure Mg ($\sim 1500 \mu\text{m}$). XRD analysis confirms the formation of Mg_2Sn and Mg_2Pb intermetallics in the produced surface alloys. Due to the availability of excess amounts of Sn and Pb during FSA, in addition to the development of supersaturated grains, intermetallics have been developed in the surface alloys. Higher hardness was recorded for the surface alloys. Polarization studies revealed lower i_{corr} values (0.99×10^{-4} and $0.78 \times 10^{-4} \text{ A/cm}^2$) for the surface alloys compared with pure Mg ($8.2 \times 10^{-4} \text{ A/cm}^2$) which is a clear demonstration of improved corrosion performance. The surface morphologies of the alloys indicated uniform corrosion due to the refined microstructure. Increased strength and higher % elongation were observed for the surface alloys; which is attributed to the benefit of the alloying. With the developed surface alloys, 2nd pass sample has shown marginally higher strength due to the uniform microstructure and decreased intermetallics compared with the 1st pass sample. Hence, it can be concluded that FSA can be successfully adapted to produce surface alloys without altering the core to improve the surface performance of the structures within the solid state. Further investigations to assess the performance of these solid-state surface alloys subjected to different working environments needed to be carried out to utilize the potential of FSA in surface engineering applications.

REFERENCES

- [1] S. Bharti, N.D. Ghetiya, K.M. Patel, Mater. Manuf. Proces. **36** (2), 135-170 (2020).
- [2] S.E. Williams, S.K. Akhil, L.I. Freddie, Int. J. Mater. Res. **107** (10) 960-969 (2016).
- [3] Y. Gao, H. Chen, J. Zhou, W. Tian, H. Nie, W. Wang, J. Liang, J. Manuf. Proces. **95** (9) 291-301 (2023).
- [4] P. Singh, C. Satish, A. Islam, S. Prasad, N. Pandit, S. Keshri, A. K. Keshri, J. Alloys Compd. **984**, 173984 (2024).
- [5] V.K. Jain, M.K. Yadav, A.N. Siddiquee, Z.A. Khan, Aust. J. Mech. Eng. **21** (5), 1489-1512 (2022).
- [6] A.P. Zykova, S.Y. Tarasov, A.V. Chumaevskiy, E.A. Kolubaev. Metals **10** (6), 772 (2020).
- [7] S. Singla, P. Sagar, A. Handa, A.S. Kang, Metallogr. Microstruct. Anal. **12**, 385-400 (2023).
- [8] B. Ratna Sunil, Int. J. Mech. Mater. Eng. **11**, 12 (2016).
- [9] J. Gandra, H. Krohn, R.M. Miranda, P. Vilaça, L. Quintino, J.F. dos Santos, J. Mater. Proces. Technol. **214** (5), 1062-1093 (2014).
- [10] J.J.S. Dilip, G.D. Janaki Ram, J. Mater. Eng. Perform. **22** (10) 3034 (2013).
- [11] J.J.S. Dilip, G.D. Janaki Ram, Mater. Charact. **86**, 146 (2013).
- [12] J.M. Rodelas, J.C. Lippold, J.R. Rule, J. Livingston, Friction stir processing as a base metal preparation technique for modification of fusion weld microstructures. [In] R.S. Mishra, W.W. Mahoney, T.J. Lienert, eds., Friction Stir Welding and Processing VI, Minerals, Metals & Materials Society (TMS), 21, (2011).
- [13] N. Balasubramanian, R.S. Mishra, K. Krishnamurthy, Int. J. Mater. Prod. Technol. **211**, 305 (2011).
- [14] R.S. Mishra, Z.Y. Ma, Mat. Sci. Eng. R **50**, 1 (2005).
- [15] B. Venkateswarlu, Sk. Shabana, Ravikumar Dumpala, B. Ratna Sunil, Int. J. Min. Met. Mater. **27**, 962-969 (2020).
- [16] B. Vandana, P. Syamala, D. Sri Venugopal, S.R.K. Imran Sk, B. Venkateswarlu, M. Jagannatham, M. Kolencik, I. Ramakanth, Ravikumar Dumpala, B. Ratna Sunil, Bull. Mater. Sci. **42**, 122 (2019).
- [17] ASTM Standard E112-12. Standard test methods for determining average grain size. West Conshohocken, PA: ASTM International; 2012. doi:10.1520/E0112-12.
- [18] F. Mansfeld, The polarization resistance technique for measuring corrosion currents. [In] Advances in Corrosion Science and Engineering, Vol 6, Plenum Press, New York, (1970).
- [19] ASTM Standard E8/E8M-11. Standard Test Methods for Tension Testing of Metallic Materials. West Conshohocken, PA: ASTM International, USA, (2009). DOI: https://doi.org/10.1520/E0008_E0008M-11
- [20] P. Ghosh, M. Mezbahul-Islam, M. Medraj, Calphad **36**, 28-43 (2012).
- [21] P.N. Alekseev, A.L. Shimkevich, I.Y. Shimkevich, WIT Trans. Modelling Simu. **59**, 343-353 (2015).
- [22] P. Hemendra, Ravikumar Dumpala, B. Ratna Sunil, Trans. Ind. Inst. Met. **71** (4), 951-959 (2018).
- [23] G.V.V. Surya Kiran, K. Hari Krishna, Sk. Sameer, M. Bhargavi, B. Santosh Kumar, G. Mohana Rao, Y. Naidubabu, Ravikumar Dumpala, B. Ratna Sunil, Trans. Nonferrous Met. Soc. China **27** (4), 804-811 (2017).
- [24] M. Venkataiah, T. Anup Kumar, K. Venkata Rao, S. Anand Kumar, I. Siva, B. Ratna Sunil, Trans. Ind. Inst. Met. **72**, 123-132 (2019).
- [25] Q. Liu, X. Chen, K. Liu, V.A.M. Cristino, K.H. Lo, Z. Xie, D. Guo, L.M. Tam, C.T. Kwok, Coatings **14** (2), 222 (2024).
- [26] A.I. Alateyah, Amal Ba Qais, Mohamed M.Z. Ahmed, Yasser Zedan, Majed O. Alawad, Mohamed S. El-Asfoury, W.H. El-Garaihy, Improved corrosion resistance and mechanical properties of severely deformed ZM31 alloy. Heliyon **10** (4), e26400 (2024).
- [27] Da-Wei Li, Hui-Yuan Wang, Dong-Song Wei, Zheng-Xue Zhao, Yan Liu, Effects of Deformation Texture and Grain Size on Corrosion Behavior of Mg-3Al-1Zn Alloy Sheets. ACS Omega **5** (3), 1448-1456 (2020).
- [28] M. Avedesian, H. Baker, ASM Specialty Handbook: Magnesium and Magnesium Alloys. ASM International, USA (1999).